We are IntechOpen,
the world's leading publisher of
Open Access books
Built by scientists, for scientists

6,900
Open access books available

186,000
International authors and editors

200M
Downloads

Our authors are among the

154
Countries delivered to

TOP 1%
most cited scientists

12.2%
Contributors from top 500 universities

BOOK CITATION INDEX
CLARIVATE ANALYTICS
INDEXED

WEB OF SCIENCE™

Selection of our books indexed in the Book Citation Index
in Web of Science™ Core Collection (BKCI)

Interested in publishing with us?
Contact book.department@intechopen.com

Magnetocaloric Effects in Metamagnetic Shape Memory Alloys

Takumi Kihara, Xiao Xu, Wataru Ito,
Ryosuke Kainuma, Yoshiya Adachi,
Takeshi Kanomata and Masashi Tokunaga

Additional information is available at the end of the chapter

Abstract

Recently, metamagnetic shape memory alloys have attracted much attention as candidates for the rare-earth free magnetic refrigerants. These materials undergo the martensitic transformation (MT) at around room temperature accompanied by a significant entropy change. The application of the magnetic field at the low-temperature martensitic phase realizes the magnetic field-induced martensitic transformation (MFIMT). Through the MFIMT, the materials show an unconventional magnetocaloric effect (MCE), which is called inverse magnetocaloric effect (IMCE). In this chapter, the direct measurement system of MCE in pulsed-high-magnetic fields is introduced. With taking the advantage of the fast field-sweep rate of pulsed field, adiabatic measurements of MCE are carried out at various temperatures. Using this technique, the IMCEs of the metamagnetic shape memory alloys NiCoMnIn and NiCoMnGa are directly measured as adiabatic temperature changes in pulsed fields. From the experimental data of MCE for NiCoMnIn, the entropy of spin system in the austenite phase is estimated through a simple mean-field model. By the combination of MCE, magnetization and specific heat measurements, the electronic, lattice and magnetic contributions to the IMCE are individually evaluated. The result for NiCoMnIn demonstrates that lattice entropy plays the dominant role for IMCE in this material.

Keywords: shape memory alloys, Heusler alloys, magnetocaloric effects, specific heat, pulsed magnetic field

1. Introduction

1.1. Magnetocaloric effects and magnetic refrigeration

Magnetocaloric effect (MCE) is thermodynamically defined as a temperature change of magnetic material due to the variation of an externally applied magnetic field. This effect is a consequence of the field variation of the entropy of a material. For instance, the application of a magnetic field to a paramagnet in the adiabatic condition reduces the disorder of spins, which lowers the magnetic entropy in the material. Since the total entropy is conserved in an adiabatic condition, the lattice entropy (and the electronic entropy in case of metals) must increase by a comparable amount of the magnetic entropy decrease. Consequently, the temperature of the material increases. In the adiabatic demagnetization process, the magnetic entropy is restored from the lattice and electronic systems, and hence, the temperature of the material decreases. In the MCE measurement, the adiabatic temperature change or the isothermal entropy change as a function of applied field is the experimentally measurable quantity. Since the MCE is sensitive to the entropy change of the material at the magnetic phase transitions, it is useful to map out the magnetic phase diagram and evaluate the temperature and field variations of entropy by the combination with the specific heat measurement. The MCE is also applied to the magnetic refrigeration, which is realized by means of the cycle of adiabatic magnetization/demagnetization and heat exchange between the magnetic material and the surrounding. This technique has long been used to realize extremely low temperatures [1, 2].

In recent decades, the magnetic refrigeration based on the MCE has attracted much attention as an alternative technique to the vapor-compression cycle for the ambient temperatures, which has been triggered by the discovery of the giant MCE (GMCE) at around room temperatures [3–5]. The GMCE is first observed in $Gd_5Si_2Ge_2$, which was reported by Pecharsky and Gschneidner [3]. This material undergoes the first-order magnetic and structural phase transition at 276 K with a giant entropy change. The maximum entropy change at the transition temperature in this material is about twice larger than that of pure Gd, which is considered as a benchmark of magnetocaloric material at around room temperature. The GMCE, in this material, appears as a result of the simultaneous changes in the magnetic and lattice entropy through the first-order phase transition (FOT). Hence, the total entropy change can exceed the limit of the magnetic entropy change caused by the spin ordering. For the simultaneous change in the magnetic and lattice entropy, the strong coupling between the spin and the lattice systems is needed. For this reason, the GMCE undergoes in many cases the first-order magneto-structural phase transition [3–12].

1.2. MCEs in Ni-Mn-based Heusler alloys

$Ni_{50}Mn_{50-x}Z_x$ (Z = Ga, In, Sn and Sb) Heusler alloys have attracted a lot of attention because of the potential applications for novel rare-earth free magnetic refrigerants [13–17]. These alloys have a cubic ($L2_1$) Heusler structure with a space group of $Fm\bar{3}m$ [15]. Some of the non-stoichiometric compositions undergo martensitic transformation (MT) from a high-temperature austenitic phase (A-phase: cubic) to a low-temperature martensitic phase of reduced symmetry (M-phase: tetragonal, orthorhombic, or monoclinic) at around room temperature ($Ni_{50}Mn_{25}Ga_{25}$ is the only Ni-Mn-based Heusler alloy that shows the MT in the stoichiometric composition [18]). In these alloys, the MT temperatures (T_{MT}) and the magnetic properties in each phase strongly depend on

the Z species and its compositional ratio x [15]. The T_{MT} increases with decreasing x. In the small x region, the ferromagnetic phase appears at the Curie temperatures in both the A phase (T_C^A) and the M phase (T_C^M), respectively [15, 16, 19–21]. In addition, the partial substitution of Ni with Co enhances the exchange coupling between the spins in the alloys, which contributes to increase T_C^A and decrease T_C^M and T_{MT} [14, 22]. Ni$_{45}$Co$_5$Mn$_{36.7}$In$_{13.3}$ undergoes MT accompanied with a magnetic phase transition from a ferromagnetic A phase to a paramagnetic M phase (monoclinic). The application of an external magnetic field to the M phase realizes magnetic-field-induced martensitic transformation (MFIMT). Kainuma et al. [14] reported, for the first time, the magnetic-field-induced shape recovery by MFIMT in this material, which is called metamagnetic shape memory effect. Owing to the large magnetic-field-induced strain and the large output stress through MFIMT, Ni$_{45}$Co$_5$Mn$_{36.7}$In$_{13.3}$ is considered to be a potential magnetic actuator material [14].

In the Ni$_{45}$Co$_5$Mn$_{36.7}$In$_{13.3}$, the MFIMT occurs as it is accompanied by significant increase of entropy, whereas the applied magnetic field aligns the spins parallel to the field direction and reduces the magnetic entropy [14, 22]. This unconventional phenomenon is called the inverse magnetocaloric effect (IMCE). The IMCEs were also observed in other compositions Ni$_{50}$Mn$_{50−x}$Z$_x$ (Z = Ga, In, Sn and Sb) [13–16, 19–23]. The IMCE indicates the significant positive change in entropy through the MFIMT that exceeds the negative contribution from the spin ordering. Therefore, the individual evaluations of the electronic, lattice and magnetic entropy changes are important to elucidate the origin of such positive entropy changes at the MFIMT. In addition, the direct measurement of MCE is also important because it enables us to evaluate the magnetic part of entropy as presented in Section 4. However, numerous studies have attempted to understand the IMCE in these materials through indirect methods such as magnetization and/or specific heat, which can only reveal the total entropy change [13–17, 19–23].

There are several studies investigating adiabatic temperature change of these Heusler alloys under magnetic fields. For instance, Liu et al. [17] carried out the direct measurement of IMCEs up to 1.9 T for NiMnInCo. In their experiments, the samples undergo the MFIMT from a pure M phase to a mixed phase because the magnetic field of 1.9 T is insufficient to complete the MFIMT. In that case, the quantitative interpretation of the MCE results is difficult. Therefore, the direct MCE measurements in the wide range of temperatures and magnetic fields are crucial to provide a greater understanding of this phenomenon.

2. Thermodynamics of MCE

In this section, a brief explanation of thermodynamics of the MCE is provided (refer to Ref. [24] for more details). Let us start with the total entropy of the system $S(T, H, p)$. The total differential of $S(T, H, p)$ can be written as:

$$dS = \left(\frac{\partial S}{\partial T}\right)_{H,p} dT + \left(\frac{\partial S}{\partial H}\right)_{T,p} dH + \left(\frac{\partial S}{\partial p}\right)_{T,H} dp \tag{1}$$

Here, T, H and p denote temperature, external magnetic field and pressure, respectively. In the adiabatic and isobaric condition ($dS = 0$ and $dp = 0$), one obtains:

$$dT = -\left(\frac{\partial T}{\partial S}\right)_H \left(\frac{\partial S}{\partial H}\right)_T dH. \tag{2}$$

Since the heat capacity of a system at a constant magnetic field $C_H(T)$ is defined as $C_H(T) = T(\partial S / \partial T)_H$, the isentropic temperature change due to the variation of the magnetic field from H_1 to H_2 can be expressed as:

$$\Delta T_{ad}(H_1 \rightarrow H_2) = -\int_{H_1}^{H_2} \frac{T}{C_H(T)} \left(\frac{\partial S}{\partial H}\right)_H dH. \tag{3}$$

On the other hand, the isothermal-isobaric entropy change is given by the well-known Maxwell relation:

$$\left(\frac{\partial S}{\partial H}\right)_{T,p} = \left(\frac{\partial M}{\partial T}\right)_{H,p} \tag{4}$$

Here, M is the magnetization of a material. After integration, Eq. (4) gives

$$\Delta S_T(H_1 \rightarrow H_2) = -\int_{H_1}^{H_2} \left(\frac{\partial M(T,H)}{\partial T}\right)_H dH. \tag{5}$$

By combining Eqs. (3) and (4), the ΔT_{ad} can be expressed as:

$$\Delta T_{ad}(H_1 \rightarrow H_2) = -\int_{H_1}^{H_2} \frac{T}{C_H(T)} \left(\frac{\partial M}{\partial T}\right)_H dH. \tag{6}$$

Using Eqs. (5) and (6), ΔT_{ad} and ΔS_T can indirectly be estimated from the magnetization and specific heat measurements. Therefore, many studies employed so far use this method to evaluate the magnetocaloric properties for the several materials [3–16].

When a material undergoes magnetic phase transitions, the MCEs at the phase boundary show different behaviour between first- and second-order phase transitions. In the case of the second-order phase transition, the entropy of a material continuously and reversibly changes, and hence, Eqs. (5) and (6) can safely be used. On the other hand, the entropy discontinuously changes through an FOT, and the heat capacity becomes infinite at the transition temperature. Since the Maxwell relation is relevant only when the entropy is a continuous function of temperature and magnetic field, the direct application of the Eqs. (5) and (6) for the FOT is not allowed. Recently, several works proposed some approaches to apply the Maxwell relations to the FOTs, but it is still in debate [25–31]. Therefore, the direct measurement of MCE (ΔT_{ad}) is crucial to gain a deep insight into the entropic behaviour through the FOTs.

## 3. Direct MCE measurement system in pulsed-high-magnetic field

As described in the previous sections, the MCE measurements are of particular interest in both fundamental (investigation of the magnetic phase transitions) and applied physics (magnetic

refrigeration). Therefore, a lot of experimental techniques of the MCE measurements have been developed so far [32–37]. Recently, Kihara et al. [36] developed a direct measurement system of MCE under pulsed high-magnetic fields up to 56 T. In this section, the details of their experimental technique are provided.

Figure 1(a) shows the schematic view of the electric circuit for the pulsed field generation system. The magnetic fields are generated in the solenoid magnet coil by discharging the energy stored in the capacitor bank [38]. **Figure 1(b)** shows the time variations of the pulsed fields generated in the nondestructive magnet installed at the Institute for Solid State Physics (ISSP), the University of Tokyo. The three curves correspond to the field profiles for charging voltages of 1, 5 and 8 kV to the capacitor bank, respectively. As shown in **Figure 1(b)**, the maximum field depends on the charging voltage to the capacitor bank. The total duration of the pulsed field is about 36 ms. This fast sweep rate of the pulsed field (the maximum sweep rate is about 10^4 T/s) has an advantage to realize the adiabatic conditions.

Figures 2(a) and **(b)** show the schematic and the picture of the sample setup. The sample is shaped into the thin plate with the thickness of less than 0.1 mm to reduce the eddy current heating caused by the application of the pulsed field (in case of metallic samples). The mag-
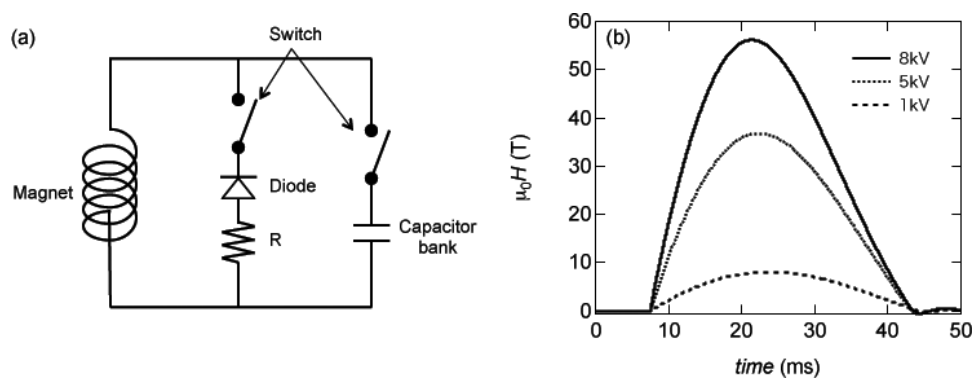

Figure 1. (a) A schematic view of the electric circuit of the pulse magnet system and (b) Magnetic field profiles of the 56-T pulse magnet at the Institute for Solid State Physics, The University of Tokyo.
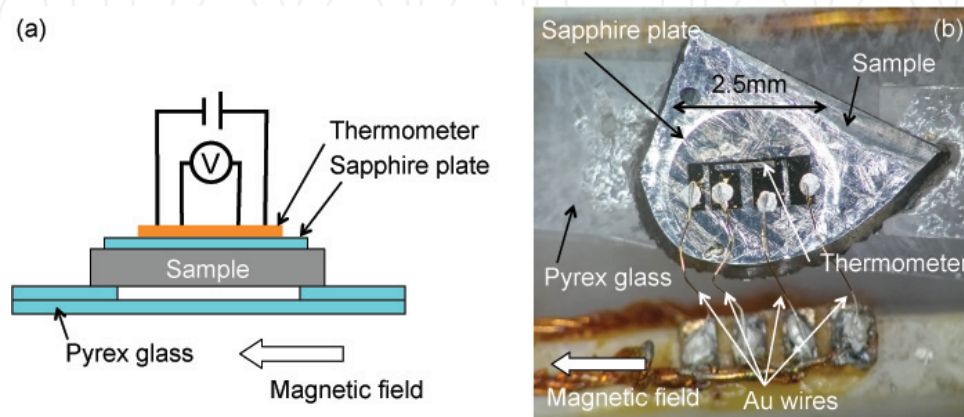
Figure 2. (a) A schematic drawing of the sample with the thermometer and (b) A picture of the sample ($Ni_{41}Co_9Mn_{31.5}Ga_{18.5}$) mounted on the MCE probe.

netic field is applied parallel to the sample plane to reduce the cross-section of the sample. In the thermometry under pulsed fields, the sample temperature changes rapidly as a function of the magnetic field. Therefore, commercial thermometers such as a Cernox® bare chip cannot be used because of the limitation of their thermal response time [35]. To detect the instantaneous change in the sample temperature in the pulsed field, a very small resistive thermometer is used, in which a patterned Au sensor (thickness: 100 nm) is deposited on a sapphire disk (thickness: 5 μm). This thermometer is mounted on top of the sample with a small amount of Apiezon® N grease as shown in **Figure 2(b)**. The small heat capacity of this thermometer (typical value is about 200 μJ/K at 300 K) and the large thermal conductance of the sapphire disk realize the fast response to the sample temperature and enable us to measure the MCEs in the pulsed fields as demonstrated for the NiCoMnIn in the next section. The sample with the thermometer is fixed on the Pyrex® glass plates, which have low thermal conductance, by the small amount of glue in order to reduce the heat leak to the surrounding. The probe (assembly of the sample, the thermometer, the sample holder, the bath heater, etc.) is inserted in the thin-walled tube made of non-magnetic stainless steel as shown in **Figure 3**. The sample space (inside of the tube) is evacuated to reduce the heat exchange between the sample and the surrounding through the residual gas. The tube is immersed in liquid helium for low temperature measurements. For high temperature measurements, small amount of helium gas is introduced into the space indicated by "Liq. He" in **Figure 3** as a heat exchange gas. During the measurement, the probe is cooled through the cold finger that is connected to the tube at the bottom of the probe. The sample temperature is regulated by the feedback operation of the bath heater (**Figure 3**). As shown in **Figure 2(b)**, the four Au wires (diameter: 30 μm) are connected to the thermometer by the small amount of Ag paste. The resistance of the thermometer is measured by the ac method using numerical lock-in technique [35, 36].
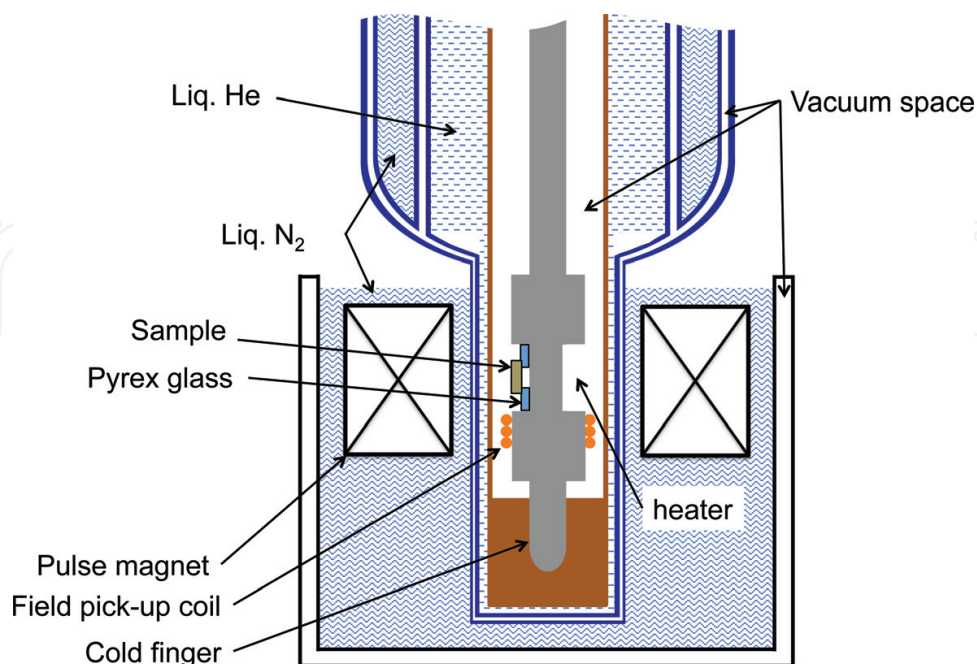

Figure 3. A schematic drawing of the probe setup.

To calibrate the Au thermometer grown on the sapphire disk, the longitudinal magnetoresistances (MRs) are measured in the pulsed fields before the MCE measurements. To carry out the isothermal measurements, the sample is removed, and the sapphire disk with the thermometer is placed directly on the Pyrex® glass substrate. Moreover, 1 atm of helium gas is introduced into the sample space at room temperature. **Figure 4** shows the MRs of the thermometer measured up to 56 T at the various temperatures (black curves). At 0 T, one can confirm the linear temperature dependence of the resistance of the metallic Au film. The slope is $dR / dT = 8.97$ mΩ/K. In the temperature region between 200 and 330 K, the Au film shows the very small MR as shown in **Figure 4**, and therefore, the linear temperature dependence of resistance can be seen in the whole field range up to 56 T. To convert the resistance to temperature, the MRs are fitted by the polynomial function of the temperature (T) and the magnetic field (H):

$$R(T, H) = a_0 + a_1 T + a_2 H + a_3 T^2 + a_4 TH + a_5 H^2 + an, \tag{7}$$

where a_n for $n = 0,1,2,…$ is the polynomial coefficient. The result of the fitting by this polynomial function for $n = 0,1,2,…,35$ is in good agreement with the data as shown by the rainbow surface in **Figure 4**. The deviation of the fitting function from the data points is within 4 mΩ over the entire range of temperatures and magnetic fields, which corresponds to the error of the temperature of 0.45 K. Hence, this Au film thermometer enables the accurate MCE measurements in the pulsed fields up to 56 T. The validity of this technique was demonstrated in the wide range of temperature through the measurements on Gd at around room temperature and on $Gd_3Ga_5O_{12}$ at low temperatures [36].
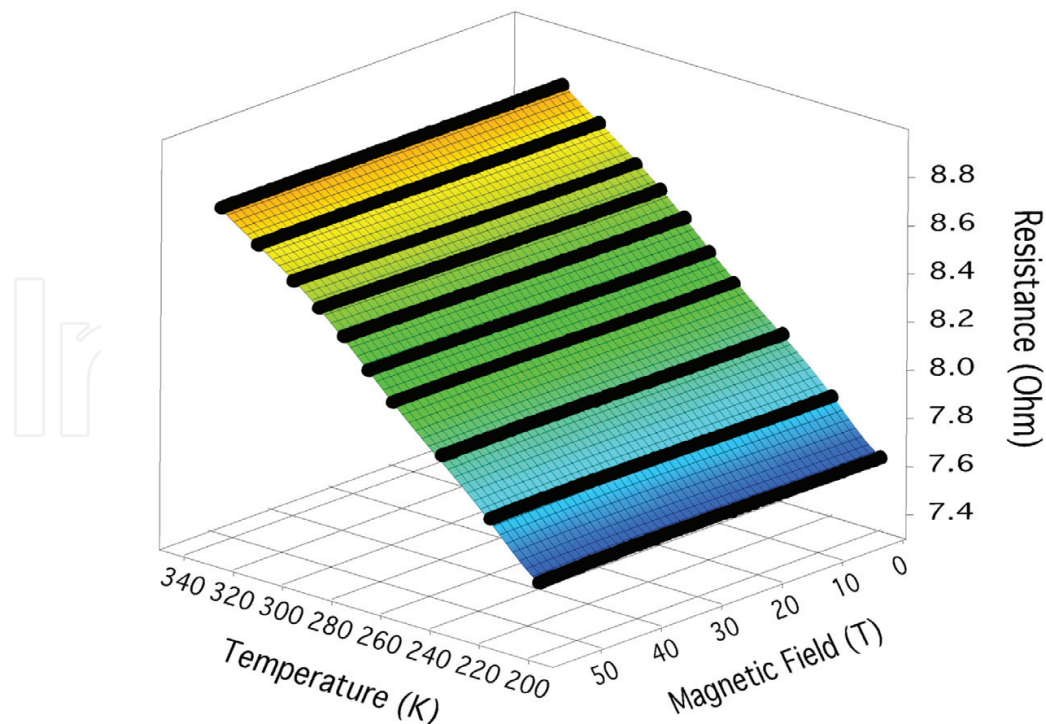
Figure 4. Magnetoresistance of the Au film thermometer deposited on a sapphire disk measured in the pulsed field up to 56 T at the various temperatures (black curves). The rainbow surface is the fitting to the polynomial function discussed in the text.

4. Magnetocaloric properties of metamagnetic shape memory alloys

4.1. Experimental procedures

In this chapter, polycrystalline samples of $Ni_{45}Co_5Mn_{50-x}In_x$ (x = 13.3 and 13.5) and $Ni_{41}Co_9$ $Mn_{31.5}Ga_{18.5}$ were used for the MCE, magnetization and specific heat measurements. The samples of $Ni_{45}Co_5Mn_{50-x}In_x$ (x = 13.3 and 13.5) were prepared by the induction melting method. The ingots were annealed at 900°C for 24 h under argon atmosphere. The samples of $Ni_{41}Co_9Mn_{31.5}Ga_{18.5}$ were prepared by the arc melting method. The ingots vacuum encapsulated in a quartz tube were annealed at 800°C for 72 h and then quenched in cold water.

Magnetization and MCE measurements were performed in pulsed-high-magnetic fields. The pulsed fields are generated by the 56-T magnet at the ISSP. The heat capacity measurements in steady fields were carried out using a thermal-relaxation method in a physical property measurement system, QuantumDesign (PPMS).

4.2. NiCoMnIn

4.2.1. Magnetization measurements

As described in Section 1.2, the metamagnetic shape memory alloy $Ni_{45}Co_5Mn_{36.7}In_{13.3}$ undergoes the MT at around room temperature. **Figures 5(a)** and **(b)** show the isothermal magnetizations of the $Ni_{45}Co_5Mn_{36.7}In_{13.3}$ measured at 310 and 280 K, respectively. The sample is in the ferromagnetic A phase at 310 K, where the M-H curve shows the ferromagnetic behaviour as shown in **Figure 5(a)**. On the other hand, as shown in **Figure 5(b)**, the magnetization increases steeply at the MFIMT, when the magnetic field is applied to the paramagnetic M phase. Here, the transition fields are defined as H_{af} for the field increasing process and H_{ms} for the field decreasing process in **Figure 5(b)**, respectively. The M-H curves measured at the various temperatures are shown in **Figure 6(a)**. One may note that the application of the pulsed-high-magnetic field up to 25 T can complete the MFIMTs in the entire temperature range. From the M-H curve at 4.2 K, the saturation magnetization moment (M_s) in the ferromagnetic A phase is estimated as M_s = 1.68 μ_B/f.u. Here, μ_B is the Bohr magneton. A formula unit (f.u.) is defined as $Ni_{0.45}Co_{0.05}Mn_{0.367}In_{0.133}$. The magnetic phase diagram of $Ni_{45}Co_5Mn_{36.7}In_{13.3}$ determined from
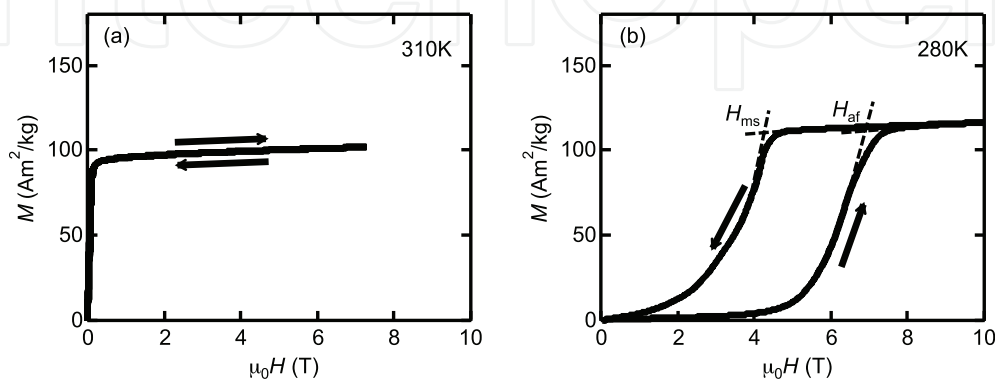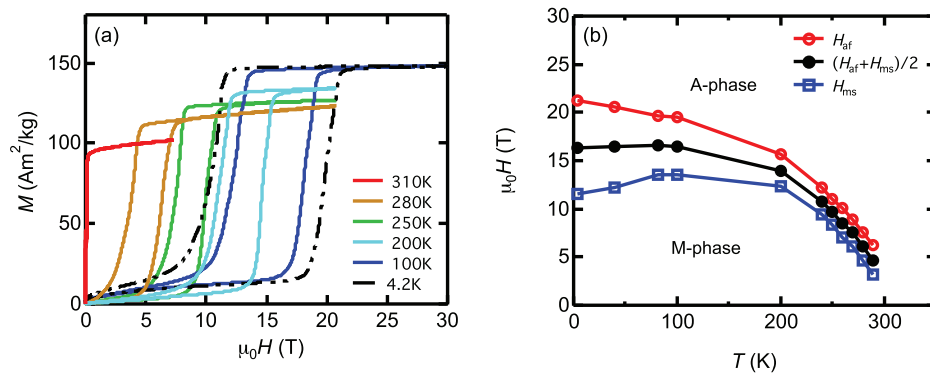

Figure 5. $M - H$ curves measured in the pulsed magnetic fields at (a) 310 and (b) 280 K for $Ni_{45}Co_5Mn_{36.7}In_{13.3}$ [39].

the $M - H$ curves is shown in **Figure 6(b)**. The $M - H$ curves and the magnetic phase diagram for $Ni_{45}Co_5Mn_{36.5}In_{13.5}$ are also provided in **Figures 7(a)** and **(b)**. Hereafter, we denote In13.3 for $Ni_{45}Co_5Mn_{36.7}In_{13.3}$ and In13.5 for $Ni_{45}Co_5Mn_{36.5}In_{13.5}$, respectively. The saturated magnetization in the ferromagnetic A phase for In13.5 is also estimated as M_s = 1.76 μ_B/f.u. As shown in **Figures 6(b)** and **7(b)** and described in Section 1.2, the magnetic phase diagram of $Ni_{45}Co_5Mn_{50-x}In_x$ is sensitive to the compositional ratio x. However, the saturated magnetizations of the two compositions are similar.

The total entropy change through MFIMT (ΔS_{tot}) can be estimated from the well-known Clausius-Clapeyron equation:

$$\mu_0 \frac{dH_0}{dT} = -\frac{\Delta S_{tot}}{\Delta M}.$$ (8)

Here, μ_0 = 4 $\pi \times 10^{-7}$ H/m is the space permeability. The ΔM is the difference of magnetization between the A and M phase. The $H_0 = (H_{ms} + H_{af}) / 2$ is used for the transition field. The results are shown in **Figure 8**, where the ΔS_{tot} is defined as the entropy change from the M to the A phase. The ΔS_{tot} at the MT temperature at the zero field is estimated to be 26 J/kg K for In13.3 and 23 J/kg K for In13.5. These values are in good agreement with that obtained from the

Figure 6. (a) $M - H$ curves measured in the pulsed magnetic fields at the various temperatures and (b) the magnetic phase diagram for $Ni_{45}Co_5Mn_{36.7}In_{13.3}$ (In13.3) [39].
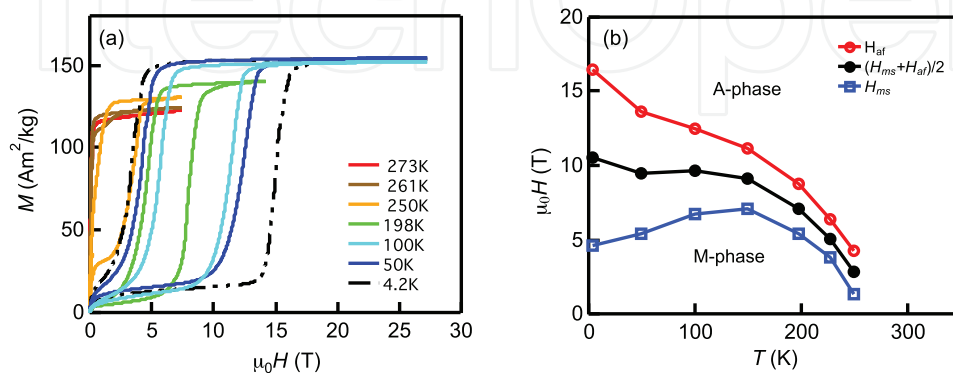
Figure 7. (a) $M - H$ curves measured in the pulsed magnetic fields at the various temperatures and (b) the magnetic phase diagram for $Ni_{45}Co_5Mn_{36.5}In_{13.5}$ (In13.5) [39].
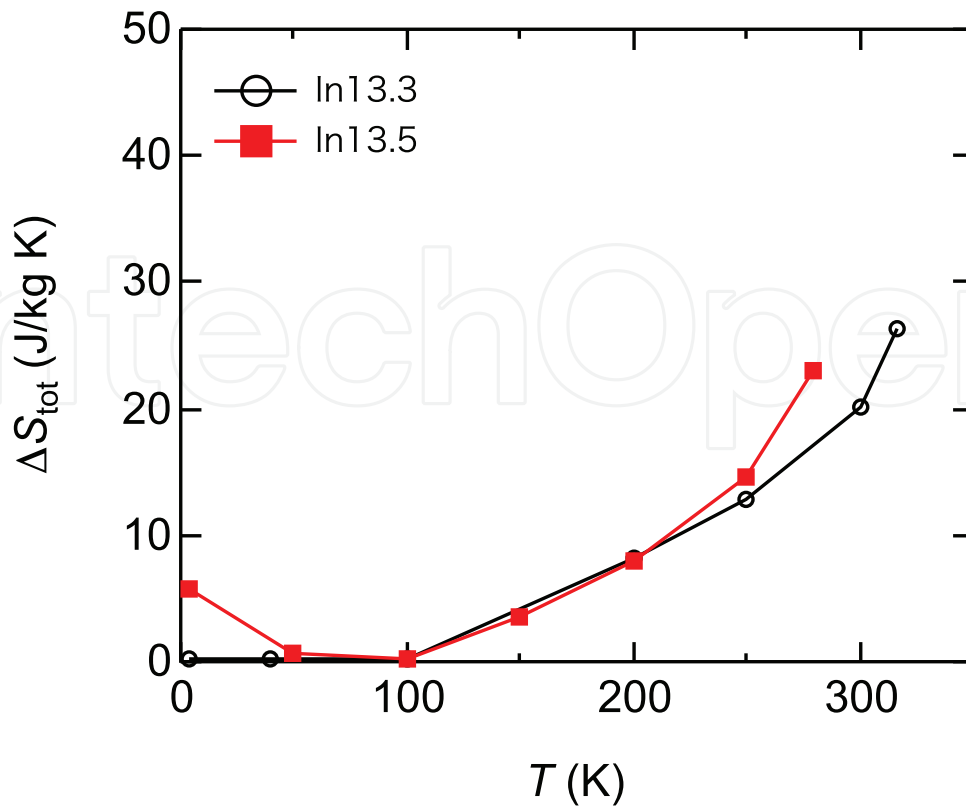
Figure 8. Temperature dependencies of the entropy change at the MFIMT estimated from the magnetic phase diagrams for $Ni_{45}Co_5Mn_{36.7}In_{13.3}$ (In13.3) and $Ni_{45}Co_5Mn_{36.5}In_{13.5}$ (In13.5) [39].

specific heat measurements [39]. The ΔS_{tot} decreases with decreasing temperature in both In13.3 and In13.5 and reaches zero at around 100 K. This indicates that the entropies of A and M phase coincide with each other below 100 K. In other words, the driving force of the MT decreases and reaches to zero below 100 K, which increases the hysteresis of the $M - H$ curves at low temperatures. The MCEs can be calculated by the $M - H$ curves using Eq. (5), which are compared with the results of direct measurements in the next section.

4.2.2. MCE measurements in the pulsed magnetic fields

The direct MCE measurement technique described in Section 3 was first applied to the In13.3 [39]. **Figures 9(a)** and **(b)** show the adiabatic changes of the sample temperature of In13.3 measured at 310 and 280 K. The typical mass of the sample for the MCE measurements is about 50 mg, which is more than 100 times larger than that of the thermometer. Therefore, we can neglect the heat capacity of the thermometer in the measurements. Since the sample is in the ferromagnetic A phase at 310 K, the conventional MCE (monotonic heating/cooling with increasing/decreasing magnetic field) due to the forced spin alignment by the applied field is observed. It is important to note that the reversible temperature change demonstrates the experimental validity: negligibly small heat exchange between the sample and the surroundings and fast response of the thermometer [36]. The result at 280 K is the MCE when the magnetic field is applied to the M phase [**Figure 9(b)**]. The steep cooling (IMCE) occurs at the MFIMT in the field-increasing process. In the successive field-decreasing process, the sample temperature heats up at MFIMT and approximately reaches to the initial temperature at the zero field as
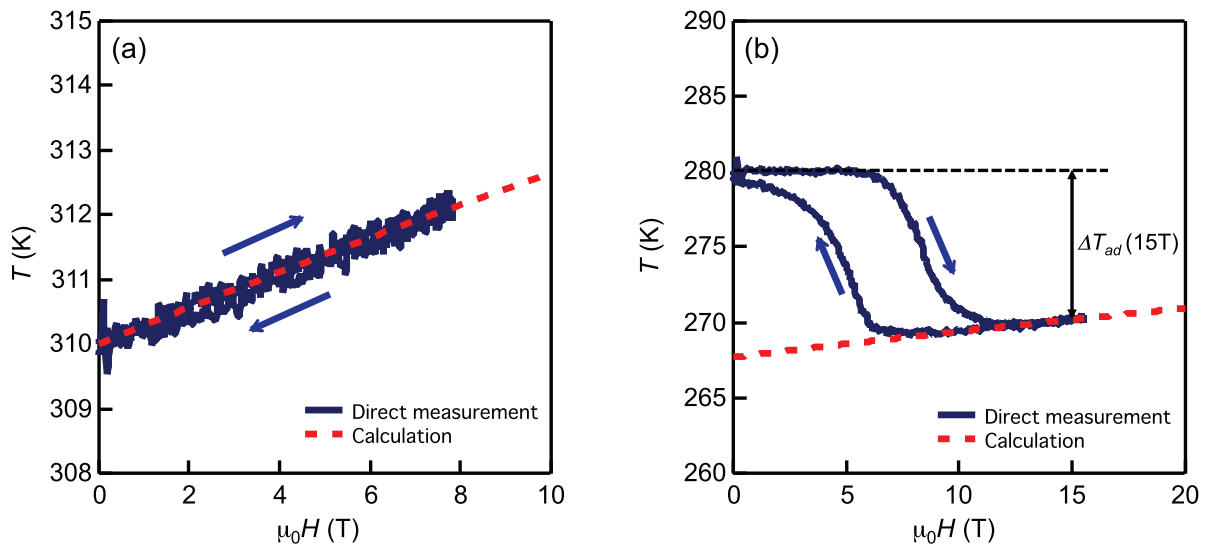
Figure 9. Magnetic field variations of the sample temperature in the adiabatic condition for In13.3. (a) The magnetic field applied to the ferromagnetic A phase and (b) the magnetic field applied to the paramagnetic M phase [39].

expected for the adiabatic measurements. The difference between the initial and final temperatures is less than 0.5 K, which indicates that the heating caused by the hysteresis loss is negligibly smaller than the MCE. In addition, a gentle slope is observed in the field-induced A phase, which is due to the change in the entropy of the ferromagnetic spins. This conventional MCE can be calculated by using the following mean-field model:

$$M(T, H) = Ng\mu_B J B_J \left(\frac{g\mu_B J \mu_0 (H - \lambda M)}{k_B T} \right). \tag{9}$$

Here, $N = 6.02 \times 10^{23}$ mol^{-1} is Avogadro's number, g is the g factor, J is the spin quantum number, $B_J(x)$ is the Brillouin function, and $k_B = 1.38 \times 10^{-23}$ J/K is Boltzmann constant. The coefficient λ represents the magnetic interaction, which is defined as $\lambda = 3k_B T_\Theta / Ng^2 \mu_B^2 J(J + 1)$ by the Weiss temperature T_Θ. Using the experimentally obtained values $g^J = 1.68$ and $T_\Theta = T_C = 387$ K, the magnetization of A phase can be calculated as a function of the temperature and magnetic field. Hence, the MCEs of A phase are calculated by this $M(T, H)$ curve through Eq. (6). The results are plotted as the red-dashed lines in **Figures 9(a)** and **(b)** and are in reasonable agreement with the experimental data. On the other hand, the MCE in the paramagnetic M phase is very small and therefore, cannot be calculated by this model.

Figure 10 shows the temperature dependence of ΔT_{ad} (15T), which is indicated in **Figure 9(b)**, the difference of the sample temperatures between 15 and 0 T as a function of the initial temperature. The ΔT_{ad} (15T) decreases linearly with increasing temperature and is in good agreement with the indirectly estimated values from the magnetization as shown in **Figure 10**.

4.2.3. Specific heat measurements

From the magnetization and MCE measurements, the total entropy change at MFIMT and the magnetic entropy in the field-induced A phase is estimated. In this section, the specific heat
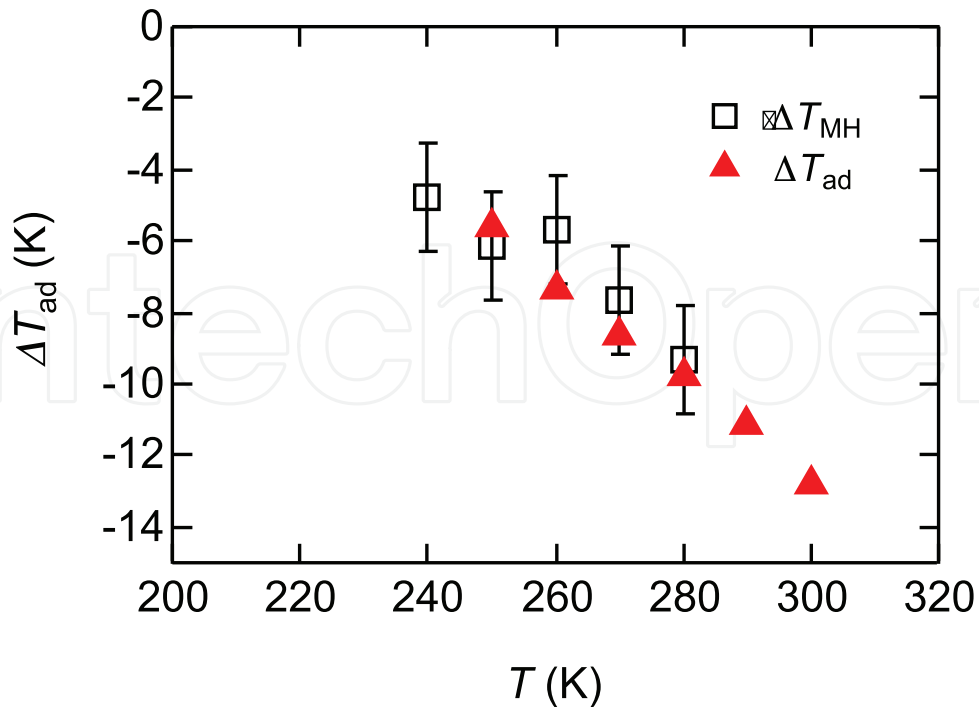
Figure 10. The temperature dependence of ΔT_{ad}(15T) (red triangles), which is defined in Figure 9(b). The open squares are the MCEs calculated from isothermal magnetization curves using Eq. (5) [39].

measurements are performed to evaluate the electronic and lattice contributions to the total entropy. As shown in **Figures 6(b)** and **7(b)**, the samples remain in the A phase at the low temperatures when they are cooled down in the magnetic field above H_{ms}. Therefore, the application of high magnetic fields enables us to measure the specific heat in both A and M phase for a sample. **Figure 11** shows the results of specific heat measurements for In13.5 at low temperatures, which are plotted as C/T versus T^2. The data of A phase (open circles) are measured after the field cooling at 12 T from room temperature. The data in both phases can be fitted by the function:

$$C = \gamma T + \beta T^3, \tag{10}$$

where the first term represents the electronic contribution and the second term corresponds to the phonon contribution. The electronic contribution to the specific heat is characterized by Sommerfeld coefficient, γ, which is proportional to the density of states at Fermi level. The phonon contribution with the coefficient β provides us with the Debye temperature Θ_D. The values [γ, Θ_D] are estimated to be [$\gamma^A = 52$ mJ/kg K^2 (3.4 mJ/mol K^2), $\Theta_D^A = 314$ K] for A phase and [$\gamma^M = 48$ mJ/kg K^2 (3.1 mJ/mol K^2), $\Theta_D^M = 361$ K] for M phase, respectively. The electronic contribution to the total entropy change ΔS_{ele} is estimated as:

$$\Delta S_{ele}(T) = (\gamma^A - \gamma^M)T. \tag{11}$$

At 300 K, ΔS_{ele} becomes 1.2 J/kg K. This value corresponds to about 5% of the total entropy change at MT. Thus, the electronic contribution to the IMCE does not play dominant role.
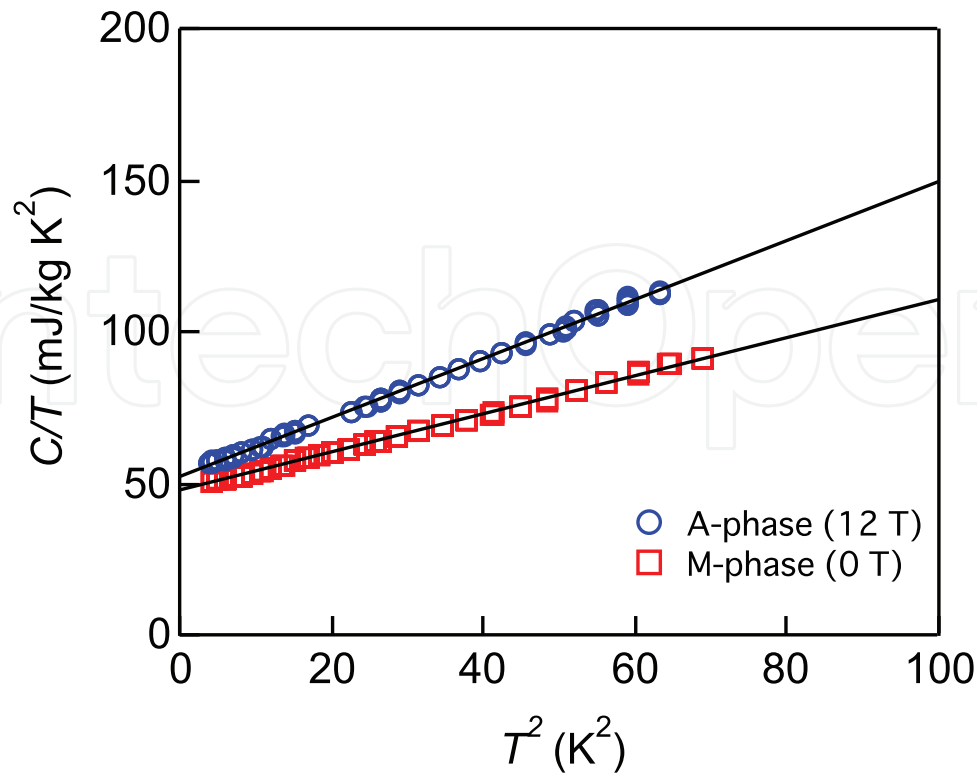
Figure 11. Specific heat of In13.5 plotted as C/T versus T^2 [39].

The specific heat of lattice system can be calculated by assuming the Debye model:

$$C_V = 9Nk_B \left(\frac{T}{\Theta_D}\right)^3 \int_0^{\Theta_D/T} \frac{x^4 e^x}{(e^x - 1)^2} dx. \tag{12}$$

Therefore, the lattice contribution to the total entropy change $\Delta S_{lat}(T)$ due to the difference of the Debye temperature between A and M phase can be calculated. Here, the C_V in Eq. (10) is the specific heat under the constant volume, while the measurements are carried out in the isobaric condition. Hence, one has to consider the difference of the specific heat between at the constant pressure and at the constant volume conditions, which can be calculated as:

$$C_p - C_V = 9\alpha^2 BVT, \tag{13}$$

where α is bulk thermal expansion coefficient, B is bulk elastic modulus, and V is molar volume. Using the values $\alpha = 6.67 \times 10^{-6}$ K^{-1} for Ni$_{45}$Co$_5$Mn$_{37}$In$_{13}$ [40] and B =140 GPa for Ni$_{50}$Mn$_{25}$In$_{25}$ [41], one obtains $C_p - C_V$ = 2.3 J/kg K at 300 K, which is smaller than the 0.6% of the experimentally obtained C_p at 300 K [39]. Therefore, the calculated data C_{lat} can be compared with the C_p for the entire temperature range. The ΔS_{lat} is calculated as 51 J/kg K at 300 K, which is about twice larger than ΔS_{tot} value obtained from the phase diagram [**Figure 7(b)**]. This indicates that the lattice contribution plays the central role in the IMCE.

4.2.4. Estimations of the electronic, lattice and magnetic entropy changes

Using Eqs. (11) and (12), ΔS_{ele} and ΔS_{lat} can be calculated for the entire temperature range, which are plotted as the blue- and green-solid curves in **Figure 12**. The magnetic entropy change ΔS_{mag} is calculated by subtracting ΔS_{ele} and ΔS_{lat} from the total entropy change ($\Delta S_{\text{mag}} = \Delta S_{\text{tot}} - \Delta S_{\text{ele}} - \Delta S_{\text{lat}}$). The T_{MT} dependence of ΔS_{mag} estimated from the experimental data of ΔS_{tot} below 300 K is plotted as the red-dashed curve in **Figure 12**. The ΔS_{mag} is estimated as $\Delta S_{\text{mag}} = -29$ J/kg K (1.9 J/mol K) at 300 K. As mentioned in Section 4.2.2, the magnetic entropy in A phase ($S_{\text{mag}}^{\text{A}}$) can be calculated by using the mean-field model. Using the values $T_C = 383$ K and $J = 0.88$ for In13.5, the $S_{\text{mag}}^{\text{A}}$ is calculated as 79 J/kg K (5.1 J/mol K) at 300 K. Therefore, the magnetic entropy of the M phase can be estimated as $S_{\text{mag}}^{\text{M}} = 108$ J/kg K (7.0 J/mol K). If one assumes a random arrangement of spins in the paramagnetic M phase, the magnetic moment of the M phase $gJ_{\text{M}} = 1.32$ is obtained from the relation: $S_{\text{mag}}^{\text{M}} = Nk_B\ln(2J_{\text{M}} + 1)$. This magnetic moment is smaller than that of the A phase by 25%. This result indicates that the magnetic contribution to the total entropy change is composed of not only the negative change due to the spin ordering but also the positive change due to the change in the magnetic moment.
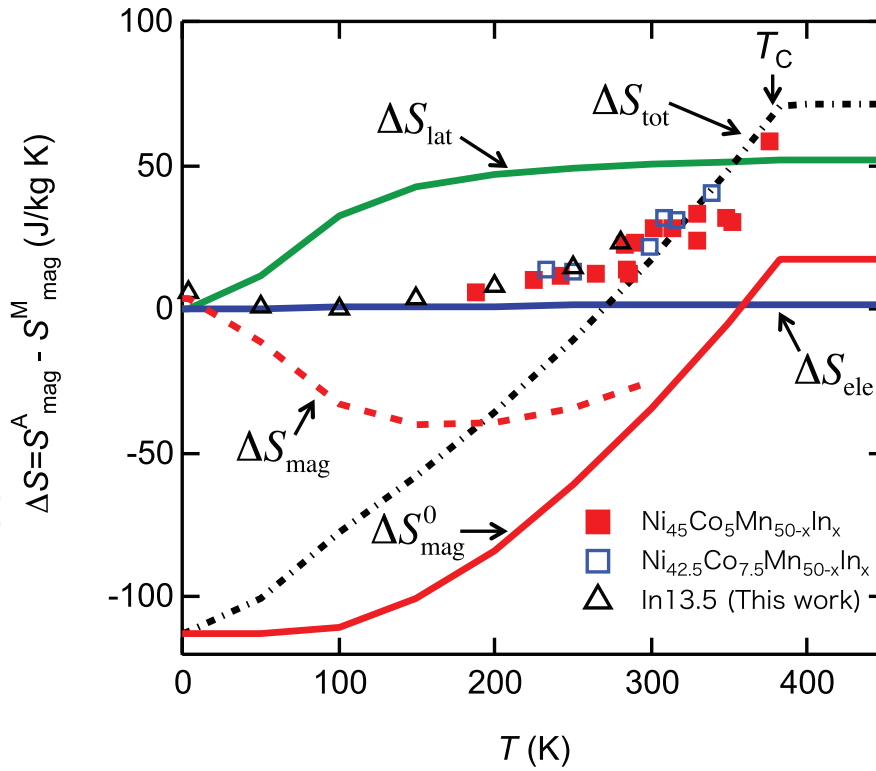
Figure 12. Calculated entropy changes through the MT as functions of the transition temperature (ΔS_{ele}, ΔS_{lat}, ΔS_{mag}, and ΔS_{tot} versus T_{MT}) [39]. The solid and open squares are the experimentally obtained ΔS_{tot} [22, 42]. The open triangles are the ΔS_{tot} estimated by the $M - H$ curves shown in Figure 7(a).

By assuming the constant value of $S_{mag}^{M} = 108$ J/kg K, the temperature dependence of the magnetic entropy change can be calculated as $\Delta S_{mag}^{0}(T) = S_{mag}^{A}(T) - S_{mag}^{M}$. The result is plotted as a red-solid curve in **Figure 12**. The calculated ΔS_{tot} is also plotted as the black-dashed curve in **Figure 12**, which coincides with the experimentally obtained data for $Ni_{50-y}Co_yMn_{50-x}In_x$ for the various x and y values above 300 K. Above T_C, the ΔS_{tot} shows the small temperature dependence. In this temperature region, both A and M phase are paramagnetic, where the contribution of the spin ordering can be neglected. Hence, the ΔS_{tot} was determined by the difference of the lattice entropy and the difference of the magnetic moment. Below T_C, the A phase is ferromagnetic, and therefore, the contribution of the spin alignment increases with decreasing T_{MT}. This effect dominates the T_{MT} dependence of the ΔS_{tot}. This behaviour of the ΔS_{tot} in the vicinity of the T_C can be confirmed in the x dependencies of the $Ni_{50-y}Co_yMn_{50-x}In_x$ [22, 43].

Below 300 K, the calculated ΔS_{tot} no longer reproduces the experimental results. This discrepancy can be attributed to the improper assumption of the constant S_{mag}^{M}. To obtain the deeper insight into the magnetic contribution to the IMCE at lower temperatures, the detailed information about the magnetic structure of M phase is necessary.

4.3. NiCoMnGa

In the NiCoMnIn, the negative entropy change due to the spin ordering through the MFIMT suppresses the ΔS_{tot} and dominates the T_{MT} dependence of the ΔS_{tot}, as shown in **Figure 12**. Therefore, the large IMCE due to the lattice entropy change and due to the change of magnetic moment is expected to occur when a material undergoes MT from the ferromagnetic/paramagnetic M phase to the ferromagnetic/paramagnetic A phase.

Recently, Kihara et al. carried out the magnetization and MCE measurements for $Ni_{41}Co_9Mn_{31.5}Ga_{18.5}$. **Figure 13** shows the isothermal $M - H$ curve measured in the pulsed magnetic field at 260 K. At this temperature, the sample is in ferromagnetic M phase at zero-field. As shown in **Figure 13**, the sample undergoes the MFIMT from the ferromagnetic M phase to the ferromagnetic A phase. In this case, it can be predicted that the negative entropy change due to the spin ordering is smaller than that when the magnetic field is applied to the paramagnetic M phase. Hence, the large and T_{MT} independent IMCE is expected to be observed.

Figure 14 shows the result of the direct MCE measurement at 257.5 K. The sample temperature increases with increasing magnetic field below 16 T in both field increasing (the M phase) and decreasing (the field induced A phase) processes. This temperature increase can be considered as the conventional MCEs due to the forced spin alignment by the magnetic field. In the field increasing process, the sample temperature steeply decreases above 16 T, which can be considered as the IMCE through the MFIMT. However, this temperature decrease is observed up to 36 T, where the MFIMT seems to be completed above 30 T according to the magnetization measurement (**Figure 13**). In the successive field decreasing process, the sample temperature increases reversibly and starts decreasing at around 25 T, where there is no anomaly in the $M - H$
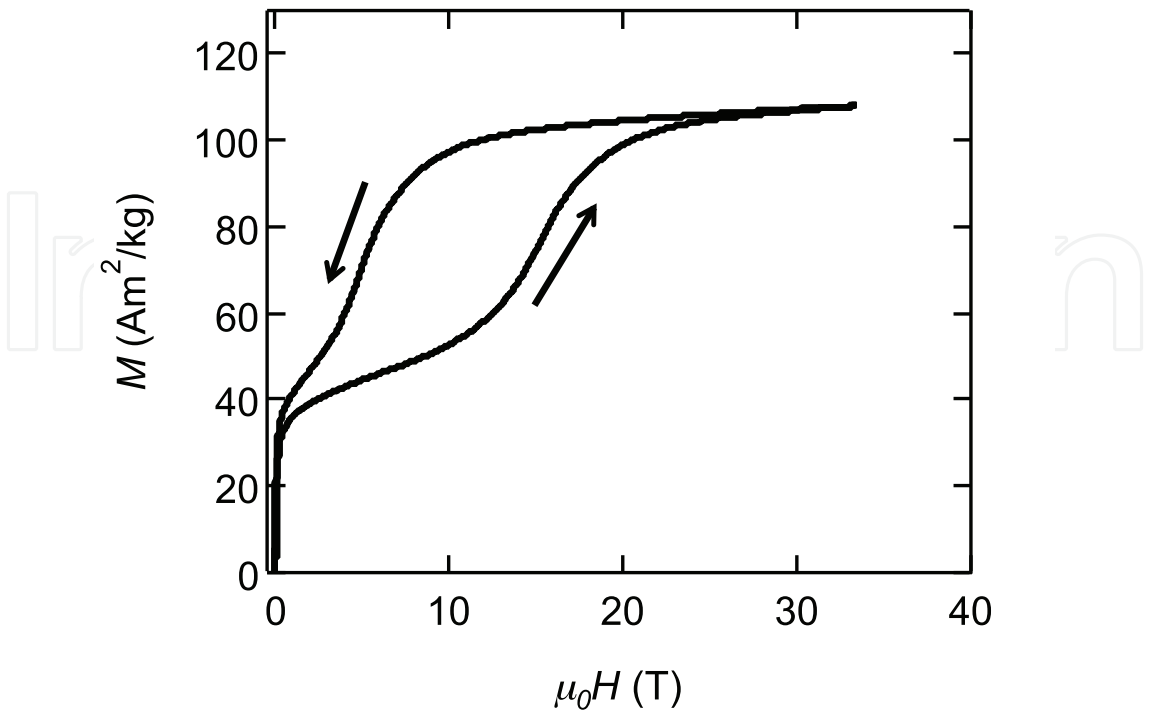
Figure 13. $M - H$ curve measured in the pulsed magnetic field at 260 K for $Ni_{41}Co_9Mn_{31.5}Ga_{18.5}$.
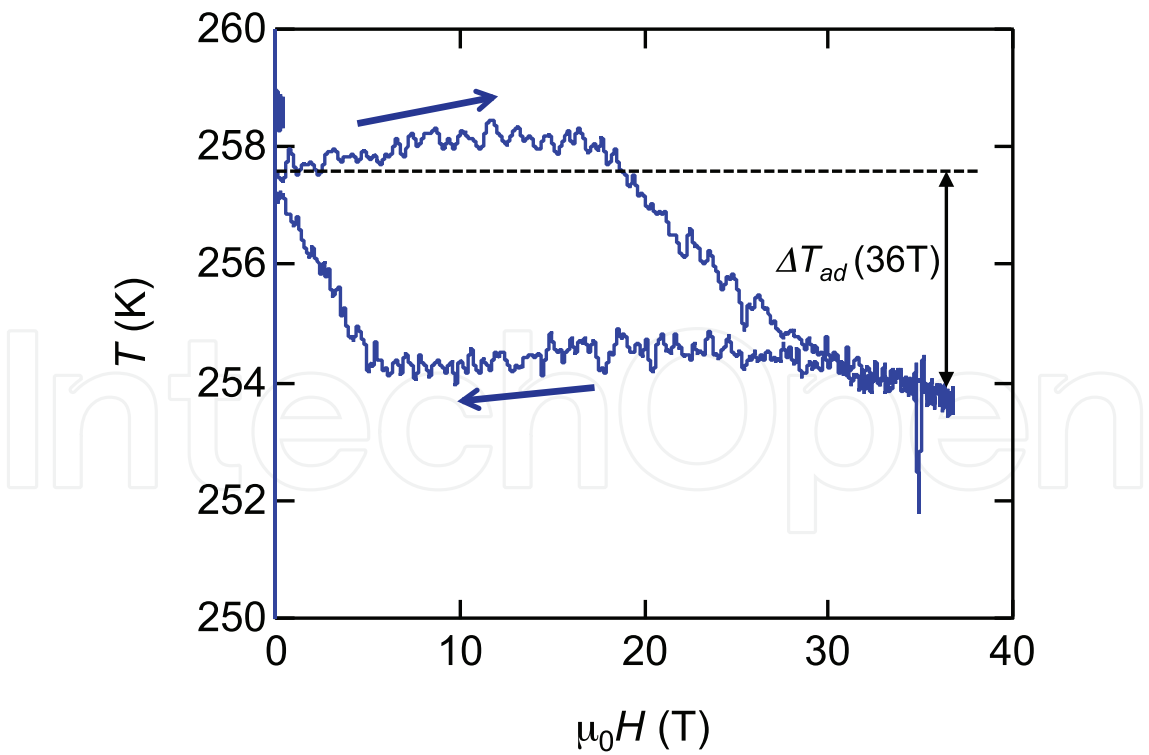
Figure 14. Magnetic field variation of the sample temperature in the adiabatic condition for $Ni_{41}Co_9Mn_{31.5}Ga_{18.5}$ measured at the initial temperature of 257.5 K.

curve. The temperature difference between 0 and 36 T is ΔT_{ad} (36T) = -3.9 K, which is indicated in **Figure 14**. Contrary to the expectation, the large IMCE is not observed. The origin of this unexpected MCE in the $Ni_{41}Co_9Mn_{31.5}Ga_{18.5}$ is still unclear.

5. Conclusion

In this chapter, the direct measurement system of magnetocaloric effect (MCE) under pulsed-high-magnetic field is introduced. Using this technique, the inverse magnetocaloric effects (IMCE) of NiCoMnIn and NiCoMnGa were measured as adiabatic temperature changes in pulsed fields. The electronic, lattice and magnetic contributions to the total entropy change through the magnetic field induced martensitic transformation (MFIMT) are individually evaluated by the combination of the results of MCE, specific heat and magnetization measurements. Through the analysis for NiCoMnIn, the validity of the present experiments for the metamagnetic shape memory alloys is demonstrated.

In conclusion, the origins of the IMCE of NiCoMnIn are as follows. The electronic contribution to the IMCE is negligibly small. On the other hand, the significant change in entropy of the lattice system plays a dominant role in the IMCE. The magnetic contribution involves the two different contributions competing with each other: the increase of magnetic moment (positive entropy change) and the spin ordering (negative entropy change). Moreover, the magnetic contribution determines the composition dependence of the total entropy change (ΔS_{tot}) at the martensitic transformation (MT), when the MT temperature (T_{MT}) and Curie temperature in the austenite phase (T_C) are close to each other. However, the model presented in this chapter cannot reproduce the composition dependence of the ΔS_{tot} when the T_{MT} and T_C are far away from each other. To clarify the origin of the IMCE for the entire temperature range, the detailed experiments about the magnetic structure of the martensitic phase are important.

The magnetization and MCE measurements are carried out at 260 K for $Ni_{41}Co_9Mn_{31.5}Ga_{18.5}$. In the MCE measurement, a complex field dependence of the sample temperature is observed. To clarify the origin of the MCE in the $Ni_{41}Co_9Mn_{31.5}Ga_{18.5}$, the MCE measurements in the wide range of temperatures and the instantaneous observation of the structural change through the MFIMT are highly desirable.

Acknowledgements

Author details

Takumi Kihara[1]*, Xiao Xu[2], Wataru Ito[3], Ryosuke Kainuma[2], Yoshiya Adachi[4], Takeshi Kanomata[5] and Masashi Tokunaga[6]

*Address all correspondence to: t_kihara@imr.tohoku.ac.jp

1 Institute for Materials Research, Tohoku University, Sendai, Japan

2 Department of Materials Science, Tohoku University, Sendai, Japan

3 Materials Science and Engineering, Sendai National College of Technology, Natori, Japan

4 Graduate School of Science and Engineering, Yamagata University, Yonezawa, Japan

5 Research Institute for Engineering and Technology, Tohoku Gakuin University, Tagajo, Japan

6 The Institute for Solid State Physics, The University of Tokyo, Kashiwa, Japan

References

[1] Debye P. Some observations on magnetization at low temperature. Annals of Physics. 1926;**81**:1154

[2] Giauque WF. A thermodynamic treatment of certain magnetic effects. A proposed method of producing temperatures considerably below 1 degree absolute. Journal of the American Chemical Society. 1927;**49**(8):1870

[3] Pecharsky VK, Gschneidner KA Jr. Giant magnetocaloric effect in $Gd_5(Si_2Ge_2)$. Physical Review Letters. 1997;**78**:4494

[4] Brück E. Developments in magnetocaloric refrigeration. Journal of Physics D. 2005;**38**:R381

[5] Gschneidner KA Jr, Pecharsky VK, Tsokol AO. Recent developments in magnetocaloric materials. Reports on Progress in Physics. 2005;**68**:1479

[6] Choe W, Pecharsky VK, Pecharsky AO, Gschneidner KA Jr, Young VG Jr, Miller GJ. Making and breaking covalent bonds across the magnetic transition in the giant magnetocaloric material $Gd_5(Si_2Ge_2)$. Physical Review Letters. 2000;**84**:4617

[7] Morellon L, Arnold Z, Magen C, Ritter C, Prokhnenko O, Skorokhod Y, Algarabel PA, Ibarra MR, Kamarad J. Pressure enhancement of the giant magnetocaloric effect in $Tb_5Si_2Ge_2$. Physical Review Letters. 2004;**93**:137201

[8] Tegus O, Bruck E, Buschow KHJ, de Boer FR. Transition-metal-based magnetic refrigerants for room temperature applications. Nature (London). 2002;**415**:150

[9] Fujieda S, Fujita A, Fukamichi K. Large magnetocaloric effect in $La(Fe_xSi_{1-x})_{13}$ itinerant-electron metamagnetic compounds. Applied Physics Letters. 2002;**81**:1276

[10] Wada H, Tanabe Y. Giant magnetocaloric effect of $MnAs_{1-x}Sb_x$. Applied Physics Letters. 2001;**58**:3657

[11] Fujita A, Fujieda S, Hasegawa Y, Fukamichi K. Itinerant-electron metamagnetic transition and large magnetocaloric effects in $La(Fe_xSi_{1-x})_{13}$ compounds and their hydrides. Physical Review B. 2003;**67**:104416

[12] Pecharsky VK, Gschneidner KA Jr. Magnetocaloric effect and magnetic refrigeration. Journal of Magnetism and Magnetic Materials. 1999;**200**:44

[13] Krenke T, Duman E, Acet M, Wassermann EF, Moya X, Mañosa L, Planes A. Inverse magnetocaloric effect in ferromagnetic Ni-Mn-Sn alloys. Nature Materials. 2005;**4**:450

[14] Kainuma R, Imano Y, Ito W, Sutou Y, Morito H, Okamoto S, Kitakami O, Oikawa K, Fujita A, Kanomata T, Ishida K. Magnetic-field-induced shape recovery by reverse phase transformation. Nature (London). 2006;**439**:957

[15] Planes A, Mañosa L, Acet M. Magnetocaloric effect and its relation to shape-memory properties in ferromagnetic Heusler alloys. Journal of Physics: Condensed Matter. 2009;**21**:233201

[16] Krenke T, Acet M, Wassermann EF. Ferromagnetism in the austenitic and martensitic states of Ni-Mn-In alloy. Physical Review B. 2006;**73**:174413

[17] Liu J, Gottschall T, Skokov KP, Moore JD, Gutfleisch O. Giant magnetocaloric effect driven by structural transitions. Nature Materials. 2012;**11**:620–626

[18] Webster PJ, Ziebeck KRA, Town SL, Peak MS. Magnetic order and phase transition in NiMnGa. Philosophical Magazine Part B. 1984;**49**:295

[19] Krenke T, Acet M, Wassermann EF. Martensitic transitions and the nature of ferromagnetism in the austenitic and martensitic states of Ni-Mn-Sn alloys. Physical Review B. 2005;**72**:014412

[20] Sutou Y, Imano Y, Koeda N, Omori T, Kainuma R, Ishida K. Magnetic and martensitic transformations of NiMnX (X = In, Sn, Sb) ferromagnetic shape memory alloys. Applied Physics Letters. 2004;**85**:4358

[21] Planes A, Mañosa L, Hennry Ehrenreich and Frans Spaepen. Vibrational properties of shape-memory alloys. In: Solid State Physics. Elsevier, Amsterdam, Netherlands; 2001. pp. 159–267

[22] Ito W, Imano Y, Kainuma R, Sutou Y, Oikawa K, Ishida K. Martensitic and magnetic transformation behavious in Heusler-type NiMnIn and NiCoMnIn metamagnetic shape memory alloys. Metallurgical and Materials Transactions A. 2007;**38A**:759

[23] Sakon T, Kitaoka T, Tanaka K, Nakagawa K, Nojiri H, Adachi Y, Kanomata T, Vadim Glebovsky. Magnetocaloric and magnetic properties of meta-magnetic Heusler alloy $Ni_{41}Co_9Mn_{31.5}Ga_{18.5}$. In: Progress in Metallic Alloys. InTech, Rijeka, Croatia; 2016. pp. 265–287

[24] Tishin AM. Magnetocaloric effect in the vicinity of phase transition. In: Buschow KHJ, editor. Handbook of Magnetic Materials. Elsevier, Amsterdam, Netherlands; 1999. pp. 395–524

[25] Pecharsky VK, Gschneidner KA Jr, Pecharsky AO, Tishin AM. Thermodynamics of the magnetocaloric effect. Physical Review B. 2001;**64**:144406-1-13

[26] Amaral JS, Amaral VS. On estimating the magnetocaloric effect from magnetization measurements. Journal of Magnetism and Magnetic Materials. 2010;**322**:1552–1557

[27] Kataoka M, Kanomata T, Umetsu RY, Kainuma R. Normal and inverse magnetocaloric effects in the ferromagnetic shape memory alloys. Journal of Magnetism and Magnetic Materials. 2014;**361**:34–43

[28] Balli M, Fruchart D, Gignoux D, Zach R. The "colossal" magnetocaloric effect in $Mn_{1-x}Fe_xAs$: What are we really measuring. Applied Physics Letters. 2009;**95**:072509-1-3

[29] Cui W, Liu W, Zhang Z. The origin of large overestimation of the magnetic entropy changes calculated directly by Maxwell relation. Applied Physics Letters. 2010;**96**:222509-1-3

[30] Tocado L, Palacios E, Burriel R. Entropy determinations and magnetocaloric parameters in systems with first-order transitions: Study of MnAs. Journal of Applied Physics. 2009;**105**:093918-1-3

[31] Liu GJ, Sun R, Shen J, Gao B, Zhang HW, Hu FX, Shen BG. Determination of the entropy changes in the compounds with a first-order magnetic transition. Applied Physics Letters. 2007;**90**:032507-1-3

[32] Kuz'min MD, Tishin AM. Magnetocaloric effect. Part 1: An introduction to various aspects of theory and practice. Cryogenics. 1992;**32**(6):545–557

[33] Levitin RZ, Snegirev VV, Kopylov AV, Lagutin AS, Gerber A. Magnetic method of magnetocaloric effect determination in high pulsed magnetic fields. Journal of Magnetism and Magnetic Materials. 1997;**170**:223–227

[34] Dan'kov SY, Tishin AM, Pecharsky VK, Gschneidner KA. Experimental device for studying the magnetocaloric effect in pulse magnetic fields. Review of Scientific Instruments. 1997;**68**(6):2432–2437

[35] Kohama Y, Marcenat C, Klein T, Jaime M. AC measurement of heat capacity and magnetocaloric effect for pulsed magnetic fields. Review of Scientific Instruments. 2010;**81**:104902-1-13

[36] Kihara T, Kohama Y, Hashimoto Y, Katsumoto S, Tokunaga M. Adiabatic measurements of magneto-caloric effects in pulsed high magnetic fields up to 55 T. Review of Scientific Instruments. 2013;**84**:074901-1-7

[37] Kohama Y, Hashimoto Y, Katsumoto S, Tokunaga M, Kindo K. Heat-pulse measurements of specific heat in 36 ms pulsed magnetic fields. Measurement Science and Technology. 2013;**24**:115005

[38] Kindo K. 100 T magnet developed in Osaka. Physica B. 2001;**294–295**:585–590

[39] Kihara T, Xu X, Ito W, Kainuma R, Tokunaga M. Direct measurements of inverse magnetocaloric effects in metamagnetic shape-memory alloy NiCoMnIn. Physical Review B. 2014;**90**:214409-1-6

[40] Li Z, Jing C, Zhang HL, Yu DH, Chen L, Kang BJ, Cao SX, Zhang JC. A large and reproducible metamagnetic shape memory effect in polycrystalline $Ni_{45}Co_5Mn_{37}In_{13}$ Heusler alloy. Journal of Applied Physics. 2010;**108**:113908-1-4

[41] Qawasmeh Y, Hamad B. Investigation of the structural, electronic, and magnetic properties of Ni-based Heusler alloys from first principles. Journal of Applied Physics. 2012;**111**: 033905-1-6

[42] Kustov S, Corró ML, Pons J, Cesari E. Entropy change and effect of magnetic field on martensitic transformation in a metamagentic Ni-Co-Mn-In shape memory alloy. Applied Physics Letters. 2009;**94**:191901-1-3

[43] Gottshall T, Skokov KP, Benke D, Gruner ME, Gutfleisch O. Contradictory role of the magnetic contribution in inverse magnetocaloric Heusler materials. Physical Review B. 2016;**93**:184431-1-5